

Enhancing Regrasping Efficiency Using Prior Grasping Perceptions with Soft Fingertips

Qiyin Huang, Ruomin Sui, Lunwei Zhang, Yenhong Zhou, Tiemin Li and Yao Jiang, *Member, IEEE*

Abstract—Grasping the same object in different postures is often necessary, especially when handling tools or stacked items. Due to unknown object properties and changes in grasping posture, the required grasping force is uncertain and variable. Traditional methods rely on real-time feedback to control the grasping force cautiously, aiming to prevent slipping or damage. However, they overlook reusable information from the initial grasp, treating subsequent regrasping attempts as if they were the first, which significantly reduces efficiency. To improve this, we propose a method that utilizes perception from prior grasping attempts to predict the required grasping force, even with changes in position. We also introduce a calculation method that accounts for fingertip softness and object asymmetry. Theoretical analyses demonstrate the feasibility of predicting grasping forces across various postures after a single grasp. Experimental verifications attest to the accuracy and adaptability of our prediction method. Furthermore, results show that incorporating the predicted grasping force into feedback-based approaches significantly enhances grasping efficiency across a range of everyday objects.

Index Terms—Perception for grasping and manipulation, grasping, contact modeling, force and tactile sensing.

I. INTRODUCTION

THE ability to grasp objects is crucial for enabling a wide range of in-hand manipulations. A successful grasp requires applying the right amount of force to lift an object off the ground without causing slippage between the fingers and the object [1]. In situations where the applied force is insufficient, the fingers may fail to provide the required force, leading to potential object slippage and unintended drops. On the other hand, excessive force can result in unwanted deformation or even damage, particularly with delicate items such as fruits and vegetables [2], [3].

When the current grasp is inadequate for the upcoming task, a regrasp is necessary. During the regrasping process, adjustments to the grasping pose are made to meet the task requirements. For instance, in the context of tool reuse, it may be necessary to grasp from different positions; in pick-and-place tasks, if the initially selected grasping pose is

This work was supported in part by the National Natural Science Foundation of China under Grant 52375017; in part by the National Natural Science Foundation of China under Grant 52175017; and in part by the Joint Fund of Advanced Aerospace Manufacturing Technology Research under Grant U2017202.

Qiyin Huang, Ruomin Sui, Lunwei Zhang, Tiemin Li, and Yao Jiang are with the Institute of Manufacturing Engineering, Department of Mechanical Engineering, Tsinghua University, Beijing 100084, China (e-mail: huangqy21@mails.tsinghua.edu.cn; ruomins@foxmail.com; zlw21@mails.tsinghua.edu.cn; zhouyanh23@mails.tsinghua.edu.cn; litm@mail.tsinghua.edu.cn; jiangyaonju@126.com).

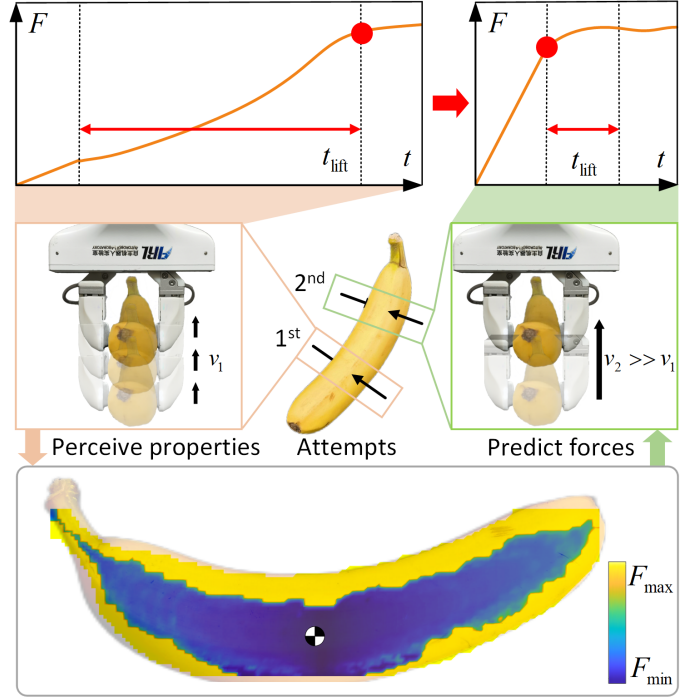


Fig. 1. During the first successful grasping, the contact information is continuously and carefully monitored and the grasping force is adjusted accordingly. After slowly lifting the unknown object, its center of gravity is measured. In regrasping attempts, the required grasping force for different positions can be directly predicted before lifting the object. This approach eliminates the need for cautious lifting with continuous feedback, thereby improving grasping efficiency.

suboptimal, a change in pose is required for regrasping; and during the handling of a batch of goods, variations in environmental occlusions may necessitate grasping the objects from different poses. Changes in the grasping pose vary the grasping forces. At the same time, information regarding the object's weight, shape, and friction coefficient remains unknown. These two factors significantly increase the difficulty of controlling grasping forces during regrasping.

Feedback-based force control methods have been widely applied in object grasping [4], [5], particularly during the initial grasp of unknown objects. These methods rely on continuously perceiving real-time feedback to control the grasping force [6]. Regrasping attempts might include variations in grasping postures, thereby altering the force requirements. Consequently, conventional feedback-based methods cautiously adjust the grasping force, treating each regrasping attempt of the same

unknown object as if it were the first. When consistently interacting with the same object, certain perceptible information remains unchanged or can be reused, even with variations in grasping postures. Unfortunately, these control strategies tend to overlook this valuable information, treating repeatedly grasped objects as if they had never encountered before. As a result, they adjust the grasping force solely based on current feedback during each attempt, which may limit overall grasping efficiency.

Predictive methods, on the other hand, emphasize extracting essential, reusable insights from prior perception. This extracted information is used to predict subsequent grasping requirements, thereby reducing reliance on real-time and overly cautious feedback during grasping process. In particular, when the prediction of grasping force becomes sufficiently accurate, it becomes feasible to directly employ the predicted grasping force for successful grasping. Leveraging and integrating this predictive method into force control strategy holds the potential to significantly improve their grasping stability and efficiency.

Our objective is to improve grasping efficiency using the perception obtained in prior grasping attempts. We initially presented a method to improve efficiency by integrating prediction into the grasping process. Analyzing the general reach-lift process revealed the significant impact of the “lift” phase on grasping efficiency. We identified how the “lift” phase can be optimized through prediction. This optimization resulted in improved grasping efficiency after the first successful grasping. Subsequently, we developed a method for predicting grasping force that accounts for soft fingertip contact and asymmetric objects, validating the accuracy of these predictions through experimental testing. Ultimately, our comprehensive experiments verified the effectiveness and applicability of the method in enhancing grasping efficiency.

The contributions of this paper are:

- 1) Identifying the “lift” phase as the primary process affecting the grasping efficiency in the general reach-lift process, and outlining methods to optimize this phase;
- 2) Proposing an efficient algorithm to determine the potential slip states and required grasping force considering the soft fingertip contact and asymmetric object;
- 3) Developing a method to improve the efficiency of re-grasping unknown objects without affecting the previous grasping process.

II. RELATED WORK

A. Grasp Force Control

Force control is a crucial aspect of robot grasping. Inspired by human grasping perception and control strategies [1], current methods predominantly employ feedback-based control strategies. These approaches require real-time monitoring of stick surfaces [7], friction coefficient [8] or other relevant metrics [9], [10] to evaluate and adjust the grasping force.

Considering that one of the primary goals of grasping force control is to prevent object slippage, slip detection serves as a widely employed intermediate indicator for grasping force control [11]. Traditional methods for identifying slip states

include neural network classification [12] or incipient slip monitoring [13]. A straightforward method to prevent slips is to increase the grasping force upon detecting proximity to slippage. However, because slippage and grasping failures often occur simultaneously, feedback-based methods typically require careful strategies and higher feedback frequencies to ensure successful grasping [14]. Moreover, slip detection requires real-time acquisition of extensive contact information, imposing high demands on sensor capabilities and feedback frequency [15].

Prediction plays a pivotal role in human grasping strategies [16]. Humans’ ability to anticipate the object properties before the grasping process begins allows for applying an appropriate amount of grasping force from the outset [17], thereby enhancing grasping efficiency. Furthermore, predicting the successful grasping force before slippage occurs can further improve the reliability of grasping, ensuring a higher success rate.

Current research has employed predictive approaches using tactile information to predict the success rate of grasping before the actual grasp, demonstrating that utilizing tactile feedback can significantly increase the success rate of grasping various objects [18]. However, these studies primarily concentrate on the ultimate outcome of object grasping, such as whether it is lifted off the ground. They often overlook critical factors like rotational sliding between the object and fingers or variations in object postures. Additionally, many of these methods primarily consider rigid fingers, simplified object shapes and neglect the contact characteristics of soft fingertips. These factors collectively restrict the applicability of these prediction methods in various scenarios.

The core of controlling grasping force based on slippage prevention lies in ensuring that the grasping force surpasses the minimum successful grasping force required to prevent slippage. Building upon this concept, this paper proposes a method for modeling and solving the minimum successful grasping force applicable to soft fingers and asymmetric objects, along with outlining the basic sensor perception requirements. We use the minimum required grasping force obtained as a reference point to regulate the grasping force. Additionally, we use force prediction to improve grasping efficiency after the first grasping.

B. Grasp Contact Modeling

In the rigid contact model, the finger can exert normal and tangential forces on the object solely through the contact point. Employing the Coulomb friction model, the frictional cone typically delineates the boundaries of tangential forces, constrained by a limited normal force and a specified frictional coefficient [19], [20].

Conversely, in the context of soft contact, the contact surface introduces a torsional moment about the contact normal. Here, the conventional frictional cone becomes inadequate, and the widely used approach shifts to the use of a limit surface. This surface illustrates the boundaries of the resultant tangential force and torsional torque [21]. The limit surface is constructed based on the power-law equation and the pressure distribution. The power law equation gives the relationship between the

radius of the contact surface and the normal force for the soft fingers [22]. Combined with the pressure distribution within the contact surface, an approximate elliptical curve can be obtained, and each point on the curve represents the limit torque under different tangential forces under a given normal force. The versatility and intuitive nature of the limit surface method make it extensively adopted and refined for different soft materials [21], [23], [24].

While the limit surface effectively reveals force-moment correlations on soft contact surfaces, it focuses on the contact analysis of individual fingers and fails to describe the overall finger-object contact system. The work by Costanzo et al. [25] has advanced the application of the limit surface theory in two-finger manipulation. They conducted an in-depth analysis and resolution of the concepts related to the instantaneous center of rotation, successfully enabling force control for dexterous pivoting of planar objects using only two fingers. In this paper, we aim to extend the limit surface theory to more general asymmetric grasping scenarios, specifically where the two-finger contacts are asymmetric, resulting in non-simultaneous sliding of the fingers. Additionally, the limit surface theory introduces more unknowns and nonlinear relationships into the system, posing challenges in calculation convergence and efficiency. To mitigate these issues, we conducted modeling of the grasping system and optimized the solution process using mathematical transformations and physical approximations.

III. PROBLEM STATEMENT

The research goal of this paper is to enhance the efficiency of regrasping by optimizing the force control process for unknown objects. For the purpose of this study, it is assumed that the gripper has already reached the required grasping position, allowing the focus to be on optimizing force control. The aim is to minimize the impact of continuous cautious feedback on grasping efficiency. The proposed method involves gathering sufficient object information during the first grasp of an unknown object to optimize the force control in subsequent regrasping attempts. The approach accounts for variations in the position and posture of the object during regrasping compared to the first grasp. Additionally, to enhance adaptability, the method must account for grasping scenarios with asymmetric contact, which may arise from factors such as object asymmetry or non-horizontal grasping postures.

A. Definitions and Assumptions

A fundamental requirement in grasping is maintaining the grasping force within the range bounded by the maximum safe grasping force (to avoid object damage) and the minimum force required for successful grasping (to prevent finger-object slippage). Considering the variable strength of different objects, a prudent approach is controlling the grasping force to exceed the minimum successful grasping force by a certain margin [26], [27]. In light of these considerations, we establish the minimum required grasping force for preventing finger-object slippage as a reference point for control and optimization. Here grasping force is defined as the force applied by the motors to bring the fingers inward for grasping.

TABLE I
LIST OF NOTIFICATIONS.

Reference Frames	
$\{\mathbb{G}\}$	gripper reference frame
$\{\mathbb{C}_i\}$	reference frame of contact surface i
Parameters and Variables	
\mathbf{W}_{req}	required wrench in $\{\mathbb{G}\}$
\mathbf{F}_{req}	required force in $\{\mathbb{G}\}$
\mathbf{M}_{req}	required moment in $\{\mathbb{G}\}$
\mathbf{F}_{ext}	external force in $\{\mathbb{G}\}$
\mathbf{M}_{ext}	external moment in $\{\mathbb{G}\}$
$\tilde{\mathbf{F}}_i$	feedback force of contact surface i in $\{\mathbb{C}_i\}$
$\tilde{\mathbf{M}}_i$	feedback moment of contact surface i in $\{\mathbb{C}_i\}$
\mathbf{r}_i	moment arms of contact surface i in $\{\mathbb{G}\}$
\mathbf{G}	object gravity in $\{\mathbb{G}\}$
\mathbf{l}	The position vector of the center of gravity of the object in $\{\mathbb{G}\}$
\mathbf{F}_i	grasping force of finger i in $\{\mathbb{G}\}$
\mathbf{F}_i^n	normal contact force of contact surface i in $\{\mathbb{G}\}$
\mathbf{F}_i^t	tangential contact force of contact surface i in $\{\mathbb{G}\}$
\mathbf{F}_i^{t1}	projected tangential contact force of contact surface i in $\{\mathbb{G}\}$
\mathbf{F}_i^{t2}	projected tangential contact force of contact surface i in $\{\mathbb{G}\}$
\mathbf{e}_i^{t1}	normalized direction vector of \mathbf{F}_i^{t1} in $\{\mathbb{G}\}$
\mathbf{e}_i^{t2}	normalized direction vector of \mathbf{F}_i^{t2} in $\{\mathbb{G}\}$
\mathbf{e}_i^x	unit vector in the x -direction of $\{\mathbb{G}\}$
\mathbf{n}_i	normalized normal vector of contact surface i in $\{\mathbb{G}\}$
\mathbf{M}_i	contact moment of contact surface i in $\{\mathbb{G}\}$
\mathbf{M}_i^n	normal contact moment of contact surface i in $\{\mathbb{G}\}$
S	slip state
\mathbf{G}_1	grasping matrix in one-finger slip state
\mathbf{G}_2	grasping matrix in two-finger slip state
$f_1(\mathbf{X}_1)$	optimization function in one-finger slip state
$f_2(\mathbf{X}_2)$	optimization function in two-finger slip state
d_c	distance between center of contact surface to the center of rotation
R	radius of contact surface
μ_i	friction coefficient of contact surface i
Material Parameters	
c	contact coefficient of soft material
γ	exponent of the power-law equation
k	coefficient of pressure distribution

Successful grasping is defined as the act of lifting an object from the ground while ensuring the object has not been crushed and there is no macro sliding between the fingers and the object. The parameters and variables are detailed in Table I. The parallel-fingers gripper holds widespread usage across industries, academia, and daily life due to its stability and structural simplicity [28], [29]. As such, this study focuses on this particular gripper type.

When the grasping position or the external forces applied to the object change, significant torsional moments from the fingers might be required to prevent slippage between the object and the fingers. The torsional moment not only requires sufficient grasping force but also relies on a substantial contact surface between the fingers and the object. This objective can be addressed by employing soft fingertips. Therefore, we adopt soft fingertips, wherein the contact transitions from point contact to surface contact. To address the required force calculation with soft contacts, we make the following assumptions:

(1) The contact surface of the object is approximately flat. Even for objects with curved surfaces, the error introduced

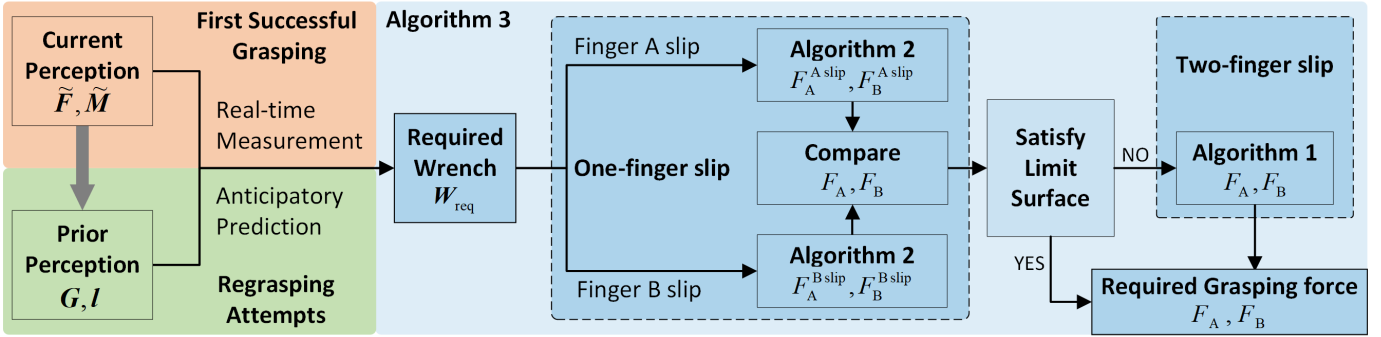


Fig. 2. Our framework designed to determine the required grasping force in both the first successful grasping and the regrasping attempts. The required wrench can be derived from current perception during the first successful grasping or from prior perception during subsequent attempts. The required grasping force is then calculated using the required wrench, the friction coefficient, and the normal vector of the contact surface.

by this assumption is limited when the finger size is small or when the curvature of the contact surface is small;

(2) The friction coefficient within the contact surface remains consistent;

(3) The stiffness of the object is much higher than that of the soft finger.

B. Framework

The key to achieving efficient grasping force control lies in determining the required grasping force for an object as quickly as possible, ideally even in advance. To address this, the paper proposes a grasping force solution framework, as shown in Fig. 2. The central variable in this framework is the required wrench, which encompasses both the resultant force and moment essential for the object to counteract external forces. Based on this variable, the process of determining the grasping force is divided into two specific tasks: the method for acquiring the required wrench in different scenarios and the algorithm for calculating the grasping force given a specific required wrench.

For scene segmentation, the multiple grasping processes of unknown objects are divided into the first successful grasp and the subsequent regrasping attempts. The first successful grasp requires continuous and careful feedback to determine the required wrench in real time. In contrast, the subsequent regrasping process can leverage the experience gained from the first grasp to obtain key information about the novel object in advance, such as its weight and center of gravity. This prior knowledge allows for the prediction of the required wrench, enhancing efficiency in regrasping.

In the grasping force solution process, the input is the required wrench, and the output is the required grasping force. Given the two soft fingertips, it is crucial to identify the sliding state—whether one finger or both fingers are sliding—when the grasping force reaches the minimum required for the object. The grasping force is then determined based on this current state.

IV. PREDICTION INTEGRATION AND INFORMATION PERCEPTION

This section aims to integrate the prediction into the grasping process to improve its efficiency. An analysis of the

typical reach-lift process is conducted. The primary process influencing grasping efficiency has been identified, along with methods to optimize it through prediction. Determining the grasping force requires acquiring the wrench required by the object. Consequently, methods for measuring or predicting the required wrench are also provided.

A. Grasping Process Analysis

Achieving a successful grasping takes three distinct steps: (1) Reach: where the gripper approaches the object surface and applies a predetermined grasping force without the need for continuous monitoring of intricate contact information; (2) lift: where the gripper raises the object until it is lifted off the ground. The minimum required grasping force continuously varies due to the interaction between the object and the ground. The primary goal of force control in this phase is to continuously measure the current contact information. This information is then used to adjust the current grasping force, ensuring it remains higher than the minimum required force to avoid slippage between the object and the gripper. (3) hold: the object detaches from the ground, and it experiences a constant gravitational force and torque.

The application of grasping force can also be divided into three steps similar to the grasping process [1], as shown in Fig. 3. It is essential to note that setting the grasping force to an excessively high value to prevent slippage is not feasible, as it can potentially damage objects of unknown strength or fragility. The presence of delay and overshoot in the grasping force control system can lead to different fluctuations, causing deviations in the actual grasping force curve.

B. Prediction Integration

The three stages—“reach,” “hold,” and “lift”—affect overall grasping efficiency differently. In the “reach” phase, force control primarily adjusting to a pre-set initial grasping force. Well-developed algorithms allow for the quick application of specific grasping forces [30], resulting in minimal impact on efficiency during this phase. Similarly, in the “hold” phase, the object experiences only constant gravity and torque, leading to a stable required grasping force and reducing the need

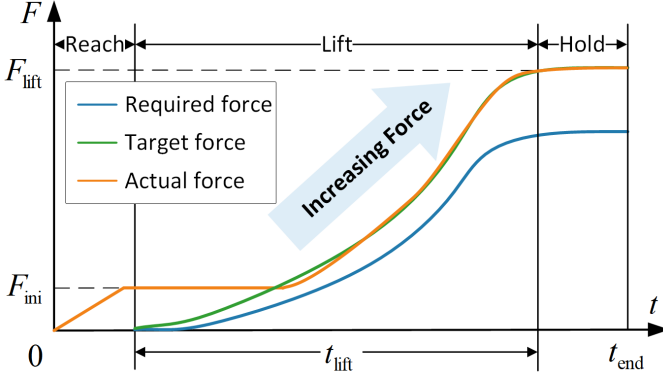


Fig. 3. Relationship between grasping force and time t , divided into three steps.

for continuous feedback, which also has a small effect on efficiency.

In contrast, the “lift” phase significantly influences grasping efficiency, as the required grasping force continuously changes due to varying ground support. The target force for control varies moment to moment, and the need for feedback complicates the process, leading to delays in sensor perception. These factors collectively result in a scenario where the gripper can only cautiously and slowly lift the object. Otherwise, the actual force does not match the required force, resulting in potential slippage.

Although predicting grasping force during the “lift” phase could enhance efficiency by reducing the need for continuous feedback, it is challenging due to unpredictable factors like ground conditions, grasping postures, and ground friction. Thus, optimizing the “lift” phase may require indirect methods.

Notably, during the “lift” phase, as ground support diminishes, the required grasping force increases, peaking when the object transitions into the “hold” phase. This peak value represents the minimum required grasping force for successful lifting. Ensuring the grasping force exceeds this value can enhance grasping success. By leveraging the predictability of the “hold” phase, this peak value can be anticipated and set as the initial grasping force, bypassing limitations imposed by cautious force control during the “lift” phase. Furthermore, in the “hold” phase, predicting grasping force can eliminate the need to estimate complex object-environment interactions.

C. Required Wrench Estimation

Estimating the required wrench for an object to counteract external forces is essential, whether using current feedback or prior perception. This estimation is used for predicting the minimum required grasping force. As illustrated in Fig. 2, current feedback is employed to estimate the required wrench during the first grasp, while prior perception is used for regrasping attempts.

The required wrench does not simply equate to the current force and torque measured by sensors. For example, when grasping a cuboid, each finger may apply substantial normal grasping forces, but gravity acting vertically downward may

not necessitate any horizontal resultant force. Consequently, summing the forces and torques from each finger can result in a calculated grasping force that is significantly higher than what the object actually needs, posing risks such as object crushing.

To address these issues, determining the required wrench for the object must involve a force balance approach. Specifically, the object requires a wrench from the fingers to counter external loads, including gravity. In other words, assessing the required wrench is equivalent to evaluating the external forces acting on the object at that moment:

$$\mathbf{W}_{\text{req}} = [\mathbf{F}_{\text{req}}, \mathbf{M}_{\text{req}}], \quad (1)$$

$$\mathbf{F}_{\text{req}} = -\mathbf{F}_{\text{ext}}, \mathbf{M}_{\text{req}} = -\mathbf{M}_{\text{ext}}, \quad (2)$$

where \mathbf{F}_{ext} and \mathbf{M}_{ext} denote the external force and moment, respectively. \mathbf{F}_{req} , \mathbf{M}_{req} , and \mathbf{W}_{req} denote the required force, moment, and wrench. Since the object is solely influenced by the fingers and the external environment, including gravity, we can directly calculate the external force and moment using sensor feedback and the principle of force and moment balance:

$$\mathbf{F}_{\text{ext}} = -(\tilde{\mathbf{F}}_A + \tilde{\mathbf{F}}_B), \quad (3)$$

$$\mathbf{M}_{\text{ext}} = -(\tilde{\mathbf{M}}_A + \tilde{\mathbf{M}}_B + \mathbf{r}_A \times \tilde{\mathbf{F}}_A + \mathbf{r}_B \times \tilde{\mathbf{F}}_B), \quad (4)$$

where $\tilde{\mathbf{F}}_A$, $\tilde{\mathbf{F}}_B$, $\tilde{\mathbf{M}}_A$ and $\tilde{\mathbf{M}}_B$ denote the forces and torques acquired from the sensor feedback, with the contact surface center as the origin. These measurements are expressed in the gripper reference frame $\{\mathcal{G}\}$. The coordinate axes of the reference frames of two contact surfaces $\{\mathcal{C}_i\}$ are aligned parallel to the coordinate axes of the gripper reference frame $\{\mathcal{G}\}$, hence the rotation matrix $\mathbf{R} = \mathbf{I}$. As a result, the forces and moments represented in both coordinate systems are numerically identical. For better clarity in subsequent equations, forces in both coordinate systems are denoted using the same expressions. The same principle applies to moments. \mathbf{r}_A and \mathbf{r}_B denote the moment arms, measured from the gripper coordinate system as the origin to the endpoints at the contact surface centers, as illustrated in Fig. 4. By substituting equations (3) and (4) into equations (1) and (2), we derive the required torque for the regrasping attempts.

In the regrasping attempts, besides the wrench applied by the fingers, an object is solely affected by gravity. When the center of mass position and the gravitational force magnitude are known, the external wrench exerted on the object can be directly computed using:

$$\mathbf{F}_{\text{ext}} = \mathbf{G}, \quad (5)$$

$$\mathbf{M}_{\text{ext}} = \mathbf{l} \times \mathbf{G}, \quad (6)$$

where \mathbf{G} denotes the gravity and \mathbf{l} denotes the position vector of the center of gravity of the object in the gripper reference frame $\{\mathcal{G}\}$. Substituting equations (5) and (6) into equations (1) and (2) yields the required torque for the regrasping attempts.

Consider that once the center of mass and the magnitude of gravity are identified, it becomes feasible to compute

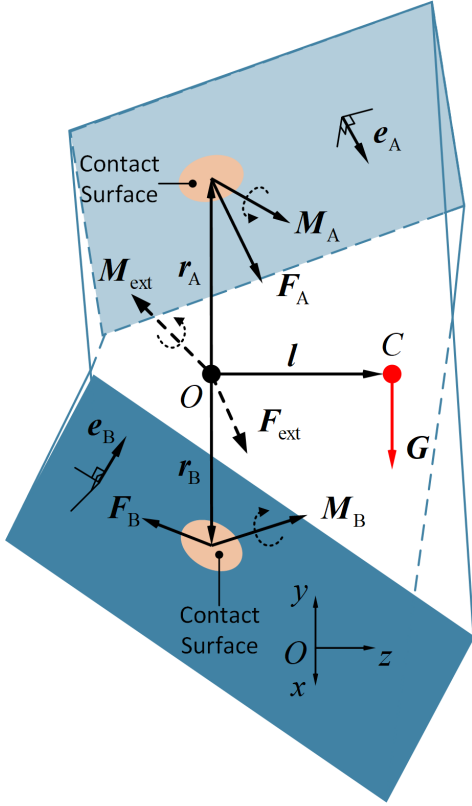


Fig. 4. Force analysis depicting contact force and other external forces acting on the object.

the required wrench for the object across various grasping positions and orientations, given the information of the relative posture between the gripper and the object. This implies that for estimating the required wrench, there is no need to grasp the object at every possible position to accumulate experience about it. Simply measuring the center of mass and gravity magnitude is adequate for estimating the wrench even for positions or orientations that have never been previously grasped.

D. Gravity Measurement

To predict the required wrench using equation (5) and equation (6), it is essential to measure the gravity of the object. When the object is not in contact with the ground, it experiences forces solely from the fingers and gravity. The torque sensed by the finger sensors and the torque induced by gravity cancel each other out. In essence, we can directly estimate the gravitational force using the feedback values from the current sensors. By combining equations (3) and (5), the gravity can be measured:

$$\mathbf{G} = -(\tilde{\mathbf{F}}_A + \tilde{\mathbf{F}}_B). \quad (7)$$

Similarly, by combining equations (4) and (6), we can obtain:

$$\mathbf{l} \times \mathbf{G} = -(\tilde{\mathbf{M}}_A + \tilde{\mathbf{M}}_B + \mathbf{r}_A \times \tilde{\mathbf{F}}_A + \mathbf{r}_B \times \tilde{\mathbf{F}}_B). \quad (8)$$

However, due to the irreversibility property of cross product, the vector \mathbf{l} cannot be directly solved for. Only the general solution of \mathbf{l} can be obtained:

$$\mathbf{l} = \mathbf{l}_0 + \gamma \mathbf{G}, \quad \gamma \in \mathbf{R}, \quad (9)$$

$$\mathbf{l}_0 = \frac{|\tilde{\mathbf{M}}_r|}{|\mathbf{G}|} \frac{\mathbf{G} \times \tilde{\mathbf{M}}_r}{|\mathbf{G} \times \tilde{\mathbf{M}}_r|}, \quad (10)$$

where $\tilde{\mathbf{M}}_r = -(\tilde{\mathbf{M}}_A + \tilde{\mathbf{M}}_B + \mathbf{r}_A \times \tilde{\mathbf{F}}_A + \mathbf{r}_B \times \tilde{\mathbf{F}}_B)$ denotes the resultant moment due to the contact forces between the finger and the object. The variable γ can take any real value, meaning that the center of gravity can move arbitrarily along the line of gravity.

Equations (9) and (10) show that each instance of sensor feedback establishes a line indicating the location of the center of gravity. When two or more non-parallel lines are obtained from separate feedback instances, their intersection can pinpoint the center of gravity. This process does not require multiple grasping attempts; instead, utilizing feedback information twice during a single grasp—by adjusting finger orientation, for example—can effectively determine the center of mass.

Integrating essential grasping information, particularly gravity and its position, into the grasping process eliminates the need for complex measurement methods or additional platforms. By leveraging the measured gravity and center of mass position, we can predict the required wrench in advance, as illustrated in Fig. 9.

V. GRIPPING FORCE SOLUTION

This chapter establishes a method for determining the minimum grasping force under a given external wrench acting on an object. Considering the soft-contact fingers and asymmetric grasping states, relying solely on equilibrium equations and limit surface constraints (see Appendix) is insufficient for efficiently solving the minimum grasping force. Specifically, the asymmetric grasp may result in non-uniform sliding of the two fingers, necessitating an assessment of the sliding conditions and the incorporation of corresponding equations for each scenario. Furthermore, the soft-contact fingers apply high-dimensional wrenches to the object, and the nonlinearities introduced by limit surface theory complicate the system's resolution. The solutions to these challenges will be detailed in this chapter.

A. Gripping Contact Modeling

Inappropriate grasping force will cause the object to slip (under a small force) or crush (above a large force). As the fragility of the object is unknown, a safe approach is to maintain the grasping force above the minimum required force by a certain margin. In other words, given a required wrench $\mathbf{W}_{\text{req}} = [\mathbf{F}_{\text{req}}, \mathbf{M}_{\text{req}}]$, we need to find the minimum required grasping force \mathbf{F}_A and \mathbf{F}_B , as shown in Fig. 5.

In the contact surface, the normal forces and frictional forces exhibit variability from one point to another, as illustrated in Fig. 6. The direction of the frictional forces depends on the relative motion between the points and the object. Consequently,

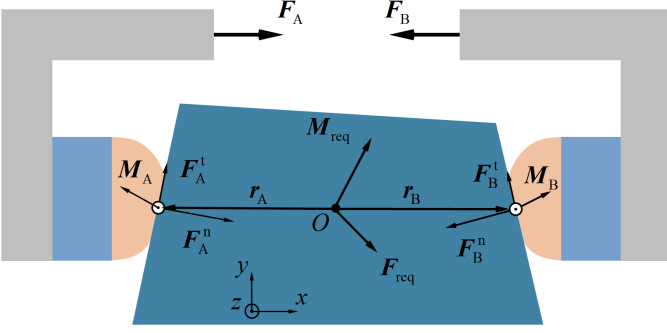


Fig. 5. Force analysis depicting the grasping force and the force and moment required by the object.

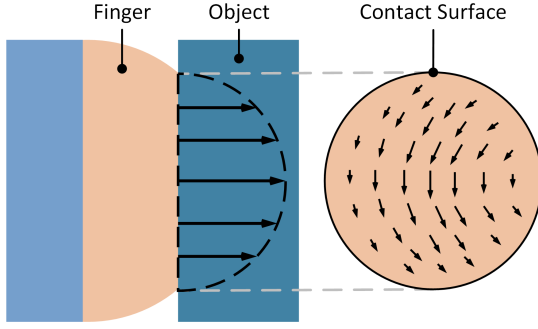


Fig. 6. Soft contact model.

calculating the maximum tangential force cannot be achieved by merely multiplying the friction coefficient with the normal force. Additionally, under soft contact conditions, distributed forces not only supply the contact force but also generate the contact moment.

When deformation is not negligible, a soft contact model should be considered, where the contact surface is no longer a single point. The forces distributed within this surface can be represented as resultant force and moment, with their points of application situated at the center of the contact surface. To analyze the forces, we project the resultant force into two components: the normal force \mathbf{F}^n and the tangential force \mathbf{F}^t . As shown in Fig. 5, the grasping forces \mathbf{F}_i and the projected contact forces \mathbf{F}_i^n , \mathbf{F}_i^t satisfy the following equation:

$$\mathbf{F}_i = \mathbf{J}_i (\mathbf{F}_i^n + \mathbf{F}_i^t), \quad (11)$$

where $i = A, B$ denotes the contact surface A or B. The matrices \mathbf{J}_i denotes the force jacobian in contact surface i . For a two-fingers parallel gripper, the force jacobians are $\mathbf{J}_A = [1, 0, 0]$ and $\mathbf{J}_B = [-1, 0, 0]$.

We align the x -axis parallel of the gripper reference frame $\{\mathbb{G}\}$ to the direction of the grasping force. The tangential forces \mathbf{F}_i^t in the contact surface A and B can be calculated as follows:

$$\mathbf{F}_i^t = \mathbf{F}_i^{t1} + \mathbf{F}_i^{t2}, \quad (12)$$

$$\mathbf{F}_i^{t1} = \mathbf{F}_i \cdot \mathbf{e}_i^{t1} = F_i^{t1} (\mathbf{n}_i \times \mathbf{e}^x) / |\mathbf{n}_i \times \mathbf{e}^x|, \quad (13)$$

$$\mathbf{F}_i^{t2} = \mathbf{F}_i \cdot \mathbf{e}_i^{t2} = F_i^{t2} (\mathbf{e}_i^{t1} \times \mathbf{n}_i), \quad (14)$$

where the tangential force \mathbf{F}_i^{t1} is parallel to the x - z plane, while \mathbf{F}_i^{t2} is parallel to the contact surface i and perpendicular

to \mathbf{F}_i^{t2} . The vector \mathbf{n}_i denotes the normalized normal vector of contact surface i . The vectors \mathbf{e}_i^{t1} and \mathbf{e}_i^{t2} denote the normalized direction vector of \mathbf{F}_i^{t1} and \mathbf{F}_i^{t2} , respectively. The vector \mathbf{e}^x denotes the unit vector in the x -direction of gripper reference frame $\{\mathbb{G}\}$.

To ensure the balance of forces and moment on the object, it is necessary to satisfy:

$$\mathbf{F}_A^n + \mathbf{F}_A^t + \mathbf{F}_B^n + \mathbf{F}_B^t = \mathbf{F}_{\text{req}}, \quad (15)$$

$$\begin{aligned} \mathbf{M}_A + \mathbf{M}_B + \mathbf{r}_A \times (\mathbf{F}_A^n + \mathbf{F}_A^t) \\ + \mathbf{r}_B \times (\mathbf{F}_B^n + \mathbf{F}_B^t) = \mathbf{M}_{\text{req}}. \end{aligned} \quad (16)$$

As shown in Fig. 5, the forces \mathbf{F}_i^n and \mathbf{F}_i^t denote the normal and tangential forces at the contact surface i . The moments \mathbf{M}_i represent the contact moment of contact surface i .

The above equations (11)–(16) alone do not suffice to solve for the grasping force. Firstly, when minimizing the grasping force, it becomes essential to ascertain the sliding states of the two fingers, i.e., whether both fingers are sliding or if only one finger is sliding. Secondly, the correlation between the torque and force provided by the contact surface when the fingers are prone to sliding has not yet been established.

B. Two-finger Slip State

When a substantial torsional force is required to be exerted by the fingers, it often leads to simultaneous slippage occurring on both fingers. When both fingers slip simultaneously, the resultant normal moment M_i^n and the resultant tangential force F_i^t satisfy the limit surface constraint, as depicted in the Appendix.

$$\begin{aligned} (F_i^t)^2 / (F_i^{t,\text{max}})^2 + (M_i^n)^2 / (M_i^{n,\text{max}})^2 = 1, \quad (17) \\ F_i^{t,\text{max}} = \mu_i F_i^n, M_i^n = M_i^{n,\text{max}}|_{d_c=0}, \end{aligned}$$

where μ_i is the friction coefficients of contact surface i , and $d_{c,i}$ is the distance between the center of rotation to the center of the contact surface.

The torque on the contact surface arises from two types of distributed forces: normal forces and tangential friction forces. As indicated by the pressure distribution (33), the normal force is symmetrically distributed, leading to a net moment of zero. Thus, the torque generated at the contact surface is primarily due to friction. Since the distributed friction forces act tangentially on the contact surface, they can only generate torque around the contact normal. Previous research suggests that while the assumption of symmetrical normal force distribution may not always hold, the resulting error is negligible [21]. Therefore, it can be assumed that the resultant moment from the fingers aligns closely with the normal to the contact surface:

$$\|\mathbf{M}_i - \mathbf{M}_i^n\| \approx 0. \quad (18)$$

Since the number of unknowns matches the number of the equation, the minimal grasping force can be solved by using (11)–(18). However, (16) and (17) are nonlinear, presenting computational efficiency and convergence challenges. To overcome this, we utilized specialized mathematical techniques and optimized the solving process.

We linearized (16) by choosing point O in Fig. 4 as the rotational center and used coordinate axes x , y , and z as the pivots. We then substituted (12)–(14), (18) into (16) and utilize the properties of the scalar triple product $(\mathbf{A} \times \mathbf{B}) \cdot \mathbf{C} = (\mathbf{B} \times \mathbf{C}) \cdot \mathbf{A}$, the scalar forms of the moment balance (16) are

$$M_{\text{req}}^x = M_A n_A^x + M_B n_B^x, \quad (19)$$

$$M_{\text{req}}^y = -F_A^n r_A n_A^z - F_A^{t1} r_A e_A^{t1,z} - F_A^{t2} r_A e_A^{t2,z} + F_B^n r_B n_B^z + F_B^{t1} r_B e_B^{t1,z} + F_B^{t2} r_B e_B^{t2,z} + M_A n_A^y + M_B n_B^y, \quad (20)$$

$$M_{\text{req}}^z = +F_A^n r_A n_A^y + F_A^{t1} r_A e_A^{t1,y} + F_A^{t2} r_A e_A^{t2,y} - F_B^n r_B n_B^y - F_B^{t1} r_B e_B^{t1,y} - F_B^{t2} r_B e_B^{t2,y} + M_A n_A^z + M_B n_B^z. \quad (21)$$

By substituting the (12)–(14) into (15), and combine (19)–(21), an underdetermined system of the equation is obtained:

$$\mathbf{G}_2 \mathbf{X}_2 = \mathbf{W}_{\text{req}}, \quad (22)$$

where $\mathbf{X}_2 = [F_A^n, F_A^{t1}, F_A^{t2}, F_B^n, F_B^{t1}, F_B^{t2}, M_A, M_B]^T$ denotes the unknown contact force and moment to be solved. The matrix $\mathbf{G}_2 \in \mathbf{R}^{6 \times 8}$ denotes the grasping matrix of two-finger slip state. The vector $\mathbf{W}_{\text{req}} = [F_{\text{req}}^x, F_{\text{req}}^y, F_{\text{req}}^z, M_{\text{req}}^x, M_{\text{req}}^y, M_{\text{req}}^z]^T$ denotes the required wrench. The solution of an underdetermined system of equations is

$$\mathbf{X}_2 = \mathbf{p}_2 + \mathbf{Z}_2 \mathbf{q}_2, \mathbf{p}_2 = \mathbf{G}_2^T (\mathbf{G}_2 \mathbf{G}_2^T)^{-1} \mathbf{W}_{\text{req}}. \quad (23)$$

The special solution \mathbf{p}_2 is the minimal norm least square solution of equation (22). Columns of \mathbf{Z}_2 are the basis vectors in the nullspace of the grasping matrix \mathbf{G}_2 . The general solution $\mathbf{q}_2 \in \mathbf{R}^{2 \times 1}$ is an unknown vector. By substituting equations (23) to the limit surface (17), a relatively simple nonlinear system of equations is obtained:

$$\mathbf{f}_2(\mathbf{X}_2) = (F_i^t(\mathbf{X}_2))^2 / (F_i^{t,\max}(\mathbf{X}_2))^2 + (M_i^n(\mathbf{X}_2))^2 / (M_i^{n,\max}(\mathbf{X}_2))^2 - 1. \quad (24)$$

Subsequently, nonlinear optimization is employed to determine the current grasping force. We utilized the classical Levenberg-Marquardt optimization method [31] to solve for the nonlinear system. To address potential issues related to multiple solutions in nonlinear systems, we initiated the search from various starting points, conducting multiple rounds of optimizations. The obtained solutions were then substituted into equation (11) to calculate the current grasping force. Among the multiple solutions, we selected the smallest real number solution as the final result. The procedural algorithm is presented in Algorithm (1).

C. One-finger Slip State

In practical grasping scenarios, there are instances where only one finger undergoes slippage. This situation is particularly noticeable when there exists a disparity in the friction coefficient or when one finger is positioned above the object and the other below, as shown in Fig. 7. When only a single

Algorithm 1: Solving Force for Two-finger Slip State.

Data: Required wrench \mathbf{W}_{req} , friction coefficient μ_i , Normal vector of contact surface \mathbf{n}_i

Result: Required force F_A, F_B

```

1 initialization;
2  $\mathbf{q}_{\text{ini}} = \{[1; 1], [1; -1], [-1; 1], [-1; -1]\}$ ;
3  $\mathbf{G}_2 \leftarrow \mu_i, \mathbf{n}_i$ ;
4  $\mathbf{p}_2, \mathbf{Z}_2 \leftarrow \mathbf{G}_2, \mathbf{W}_{\text{req}}$ ;
5 for  $k \leftarrow 1$  to 4 do
6    $\mathbf{q}_2 = \mathbf{q}_{\text{ini}}(k)$ ;
7   // Levenberg-Marquardt optimization
8   min  $\mathbf{f}_2(\mathbf{X}_2)$  subject to  $\mathbf{X}_2 = \mathbf{p}_2 + \mathbf{Z}_2 \mathbf{q}_2$ ;
9    $\mathbf{X}_2^{(k)} = \mathbf{X}_2 |_{\min \mathbf{f}_2(\mathbf{X}_2)}$ ;
10   $F_A^{(k)}, F_B^{(k)} \leftarrow \mathbf{X}_2^{(k)}$ ;
11  $F_A, F_B \leftarrow \min_k (F_A^{(k)}, F_B^{(k)})$ ;

```

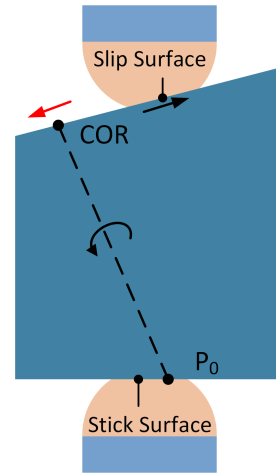


Fig. 7. Kinematic analysis of one-finger slip state.

finger slips, the contact surface of the stick finger no longer satisfies the limit surface theory equation (17), rendering Algorithm (1) inapplicable.

During one-finger slippage, an instantaneous center of rotation (COR) exists for the sliding finger (see Appendix). As the object adheres to the surface, its movement can be seen as rotation around an axis connecting the COR and a point (P0) on the stick surface. The displacement of contact points increases with their distance from the rotation axis. With relative sliding between the finger and the object, points on the contact surface lag behind, resulting in slippage. If the COR is far from the contact surface, the relative displacement between the finger and contact points increases, leading to more sliding. On the other hand, as points approach P0, the fingers can match the object's motion, preventing slippage.

As the COR moves closer to the contact surface, the displacements in the slip surface decrease, aligning more closely with those in the stick surface. When the COR is close enough to the contact surface, or even enters the contact surface, the object displacement within the slip surface may

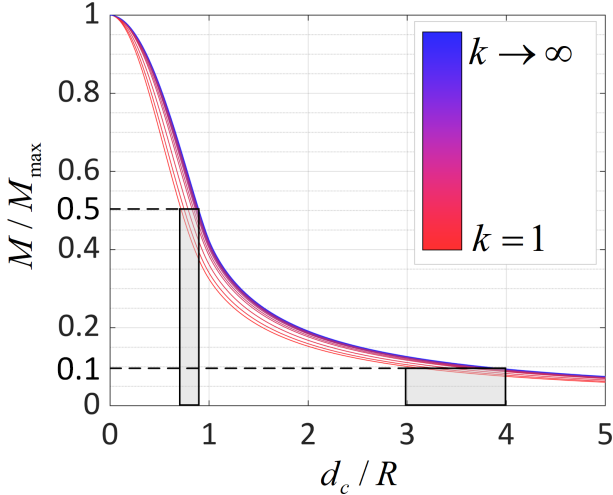


Fig. 8. The relationship between the torque exerted by the contact surface and the position of the COR for different pressure distribution coefficients k .

even be smaller than that within the stick contact surface. This unexpected reversal implies that the stick contact surface, contrary to expectations, becomes more susceptible to sliding compared to its actual sliding state. Therefore, for the one-finger sliding state, the COR of the slip surface should not be too close to the contact surface; otherwise, the stick surface will also experience sliding.

The direction of friction forces at the contact surface is influenced by the COR. When the COR is distant, the friction directions align closely, and if located at infinity, they are parallel. With a limited normal force, this alignment reduces the torque generated by the contact surface. As shown in Fig. 8, as the distance ratio d_c/R increases, the torque decreases rapidly. When the COR remains within the contact surface ($d_c/R > 1$), the torque can drop to half its maximum, and when $d_c/R > 4$, it can fall below 0.1 times its maximum value.

Our observations indicate that as d_c/R increases, the torque provided by the contact surface diminishes quickly. In light of the COR of the sliding finger moving away from the contact surface during the one-finger slip state, we adopt an approximation. This approximation assumes that the torque transmitted by the finger through the slip surface is negligible, resembling a rigid contact model. This simplified approach avoids complex material mechanics analyses and time-consuming finite element simulations. Ultimately, our solution addresses the challenge of determining grasping force during the one-finger slip state in an approximate yet effective manner:

$$\mathbf{M}_{\text{slip}}^n \approx 0, \quad (25)$$

where $\mathbf{M}_{\text{slip}}^n$ denotes the normal moment of sliding contact surface. For slip surface, the normal force $\mathbf{F}_{\text{slip}}^n$ and tangential force $\mathbf{F}_{\text{slip}}^t$ need to satisfy:

$$\mathbf{F}_{\text{slip}}^n = \mu_{\text{slip}} \mathbf{F}_{\text{slip}}^t. \quad (26)$$

We have also employed a linearization method similar to the method of the two-finger slip state. Substitute the (12)–

Algorithm 2: Solving Force for One-finger Slip State.

Data: Required wrench \mathbf{W}_{req} , friction coefficient μ_i , normal vector of contact surface \mathbf{n}_i , slip state \mathcal{S}

Result: required grasping force $F_{\text{slip}}, F_{\text{stick}}$, contact force and moment of the stick contact surface $F_{\text{stick}}^n, F_{\text{stick}}^t, M_{\text{stick}}^n$

- 1 initialization;
 - 2 $\mathbf{G}_1 \leftarrow \mu_i, \mathbf{n}_i, M_{\text{slip}}^n, \mathcal{S}$;
 - 3 $\mathbf{p}_1, \mathbf{Z}_1 \leftarrow \mathbf{G}_1, \mathbf{W}_{\text{req}}$;
 - 4 $\mathbf{X}_1 = \mathbf{p}_1 + \mathbf{Z}_1 \mathbf{q}_1$;
 - 5 // Solve for the quadratic equation $f_1(\mathbf{X}_1)$
 - 6 $\mathbf{X}_1^{(1)}, \mathbf{X}_1^{(2)} \leftarrow f_1(\mathbf{X}_1) = 0$;
 - 7 $F_i^{(1)}, F_i^{(2)} \leftarrow \mathbf{X}_1^{(1)}, \mathbf{X}_1^{(2)}$;
 - 8 $k \leftarrow \min(F_i^{(1)}, F_i^{(2)})$;
 - 9 $F_{\text{slip}}, F_{\text{stick}}, F_{\text{stick}}^n, F_{\text{stick}}^t, M_{\text{stick}}^n \leftarrow k, (\mathbf{X}_1^{(1)}, \mathbf{X}_1^{(2)})$;
-

(14) into (15), and combine (19)–(21), (25), we obtain another underdetermined system of the equation:

$$\mathbf{G}_1 \mathbf{X}_1 = \mathbf{W}_{\text{req}}, \quad (27)$$

where $\mathbf{X}_1 = [F_A^n, F_A^{t1}, F_A^{t2}, F_B^n, F_B^{t1}, F_B^{t2}, M_{\text{stick}}^n]^T$ denotes the unknowns to be solved. M_{stick}^n denotes the moment offered by the stick surface. The matrix $\mathbf{G}_1 \in \mathbf{R}^{6 \times 7}$ denotes the grasping matrix of one-finger slip state. The vector $\mathbf{W}_{\text{req}} = [F_{\text{req}}^x, F_{\text{req}}^y, F_{\text{req}}^z, M_{\text{req}}^x, M_{\text{req}}^y, M_{\text{req}}^z]^T$ denotes the required wrench. The solution of an underdetermined system of equations is

$$\mathbf{X}_1 = \mathbf{p}_1 + \mathbf{Z}_1 \mathbf{q}_1, \mathbf{p}_1 = \mathbf{G}_1^T (\mathbf{G}_1 \mathbf{G}_1^T)^{-1} \mathbf{W}_{\text{req}}. \quad (28)$$

The special solution \mathbf{p}_1 is the minimal norm least square solution of equation (27). Columns of \mathbf{Z}_1 are the basis vectors in the nullspace of the grasping matrix \mathbf{G}_1 . The general solution $\mathbf{q}_1 \in \mathbf{R}$ is the unknown to be solved. By substituting equations (28) to (26) and (12), we obtain a quadratic equation:

$$f_1(\mathbf{X}_1) = (F_{\text{slip}}^n(\mathbf{X}_1))^2 - \mu_{\text{slip}}^2 (F_{\text{slip}}^t(\mathbf{X}_1))^2. \quad (29)$$

The quadratic equation can be directly solved without the need for nonlinear optimization methods. The obtained solutions were then substituted into equation (11) to calculate the current grasping force. The smallest real number solution among the two solutions was then chosen as the obtained result of the solution. The procedural algorithm is presented in Algorithm (2).

D. Gripping Force Solution

Based on the Algorithms (1) and (2), the minimum required grasping force for both sliding states can be determined, resulting in two distinct sets of solutions. However, only one type of sliding state occurs at the point where the grasping force reaches its minimum value. Therefore, it is necessary to determine which sliding state will occur.

In the case of the one-finger slip state, only the mechanical characteristics of the slip surface were analyzed, as represented by equation (25). In practice, however, the stick surface must also adhere to specific conditions to maintain its adherence. Precisely, to sustain the stick surface, the moments and tangential forces exerted by the contact surface must not surpass the limit surface. The sliding state will transition from the one-finger slip state to the two-finger slip state if the following conditions are satisfied:

$$(F_{\text{stick}}^t)^2 / (F_{\text{stick}}^{t,\max})^2 + (M_{\text{stick}}^n)^2 / (M_{\text{stick}}^{n,\max})^2 > 1, \quad (30)$$

$$F_{\text{stick}}^{t,\max} = \mu_{\text{stick}} F_{\text{stick}}^n, M_{\text{stick}}^{n,\max} = M^n |_{d_c=0},$$

where F_{stick}^t and M_{stick}^n denote the tangential force and normal moment of the stick surface, respectively. $F_{\text{stick}}^{t,\max}$ and $M_{\text{stick}}^{n,\max}$ denote the maximum tangential force and normal moment that the stick surface can offer.

We begin by assuming a one-finger slip state and employ Algorithm (2) to compute the grasping force along with the forces and moments facilitated by the stick surface. Subsequently, an evaluation is conducted to determine whether the stick surface complies with equation (30). Satisfying this equation signifies the transition to a two-finger slip state. Algorithm (1) is then utilized to determine the current grasping force.

When dealing with a situation where only one finger slips, it is important to determine which finger slide first. This determination method requires separately computing the minimum required grasping force for the scenarios where either finger A or B undergoes sliding. If the calculated grasping force for finger A sliding surpasses that of finger B sliding, it indicates that finger A initiates the sliding action, and vice versa. This approach is employed because, as the grasping force gradually decreases, it first reaches the larger value among the solutions. At this point, the corresponding finger will start to slip, leading to the grasping failure. The overall computational procedure is outlined in Algorithm (3).

Finally, a multiple grasping framework for an unknown object is proposed, as shown in Fig. 9. Initially, during the first grasp, the current contact force and contact torque are measured, and equation (1)–(4) is used to determine the required force spinor for the object. The grasping force needed at that moment is then calculated using Algorithm (3), and the gripper’s grasping force control target is set accordingly. These steps are repeated throughout the lifting process until the object is securely grasped. After the object is successfully lifted, equation (7)–(10) is used to measure the object’s unknown center of gravity and weight. During the regrasping process, the measured object parameters are used to directly predict the required wrench after the object is lifted, using equations (5), (6). Algorithm (3) is then applied to determine the final grasping force needed to lift the object, and the grasping force control target is set to a threshold slightly higher than this value. The object is then lifted directly, eliminating the need for continuous cautious feedback during the regrasping process.

Algorithm 3: Solving Force with the required wrench.

Data: Required wrench \mathbf{W}_{req} , friction coefficient μ_i , Normal vector of contact surface \mathbf{n}_i

Result: required grasping force F_A, F_B , slip state \mathcal{S}

```

1 initialization;
2  $\{F_{\text{slip}}, F_{\text{stick}}, F_{\text{stick}}^n, F_{\text{stick}}^t, M_{\text{stick}}^n\} |_{\text{A slip}} \leftarrow$ 
   Algorithm_2 ( $\mathbf{W}_{\text{req}}, \mu_i, \mathbf{n}_i, \mathcal{S} = \text{A slip}$ );
3  $\{F_{\text{slip}}, F_{\text{stick}}, F_{\text{stick}}^n, F_{\text{stick}}^t, M_{\text{stick}}^n\} |_{\text{B slip}} \leftarrow$ 
   Algorithm_2 ( $\mathbf{W}_{\text{req}}, \mu_i, \mathbf{n}_i, \mathcal{S} = \text{B slip}$ );
4 if  $(F_{\text{slip}} + F_{\text{stick}}) |_{\text{A slip}} > (F_{\text{slip}} + F_{\text{stick}}) |_{\text{B slip}}$  then
5    $\mathcal{S} = \text{A slip}$ ;
6    $F_A, F_B \leftarrow \{F_{\text{slip}}, F_{\text{stick}}\} |_{\text{A slip}}$ ;
7 else
8    $\mathcal{S} = \text{B slip}$ ;
9    $F_A, F_B \leftarrow \{F_{\text{slip}}, F_{\text{stick}}\} |_{\text{B slip}}$ ;
10 if  $F_{\text{stick}}^n, F_{\text{stick}}^t, M_{\text{stick}}^n$  satisfy (30) then
11    $\mathcal{S} = \text{two-finger slip}$ ;
12    $F_A, F_B \leftarrow \text{Algorithm}_1 (\mathbf{W}_{\text{req}}, \mu_i, \mathbf{n}_i)$ ;

```

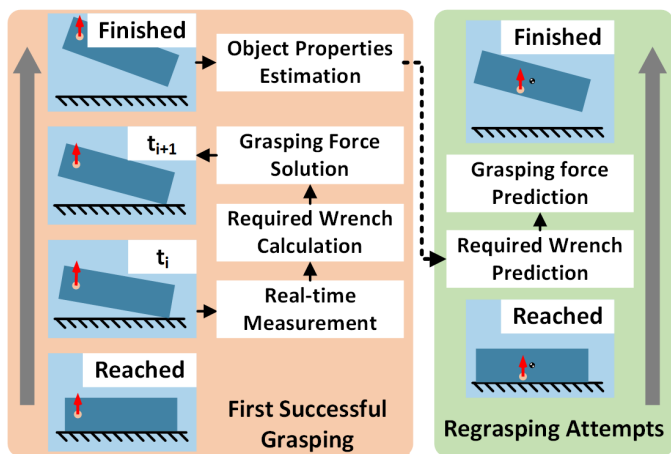


Fig. 9. Grasping process for unknown objects.

VI. EXPERIMENT

Four experiments were conducted to validate the effectiveness of the proposed method. First, we utilized two experiments to validate the accuracy and adaptability of the force prediction. Next, we integrated grasp force prediction into the grasp force control strategy and experimentally validated the effectiveness of this integration in improving grasping efficiency. Additionally, another experiment demonstrated the applicability of the prediction-integrated method across a variety of everyday objects. Finally, in a comparative demonstration, we evaluated our method against pure feedback-based approaches and another method that employs predefined constant grasping forces. This comparison confirmed the effectiveness of our approach in enhancing both grasping efficiency and success rates across multiple regrasping scenarios.

The experimental setup is depicted in Fig. 10. The robotic arm, equipped with a gripper, was fitted with the Tac3D tactile sensor on its fingertips. The Tac3D sensor features a soft

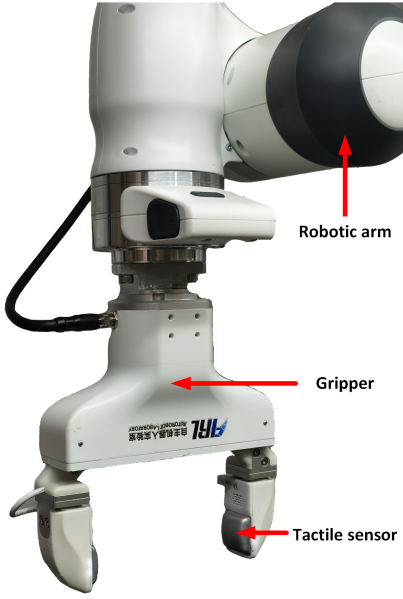


Fig. 10. Experiment platform.

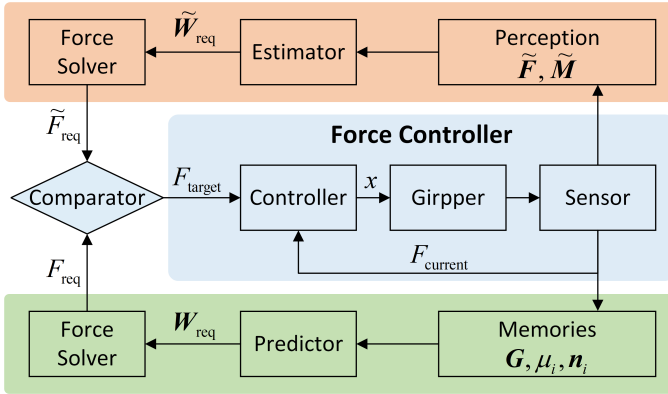


Fig. 11. Gripping force control framework. The comparator controls whether to use force prediction. The controller takes the target force F_{target} as input and the distance of finger x as the output, utilizing a well-tuned PID control.

silicone surface and, based on reference [22], is characterized by a contact coefficient $c = 2.07$, a power-law equation exponent $\gamma = 0.259$, and a pressure distribution coefficient $k = 2$. Under the experimental conditions of this study, the maximum force measurement error for the sensor is 0.1 N, and the maximum torque measurement error is 1 N-mm.

The feedback-based method and force prediction necessitate four types of information from the contact surface: the friction coefficient, surface normal, resultant force, and torque. For acquiring the resultant force and torque data from the contact surface, we opted for the Tac3D tactile sensor [32] (other 6D force-torque sensors can also be employed). Given the capability of Tac3D to measure the 3D deformation of the contact surface, it substitutes traditional vision-based methods to obtain the contact surface normal. Before lifting the object, the fingers are moved to slightly slide over the object while measuring the current tangential and normal forces at the contact surface. This data will be used to calculate the friction coefficient of the object.

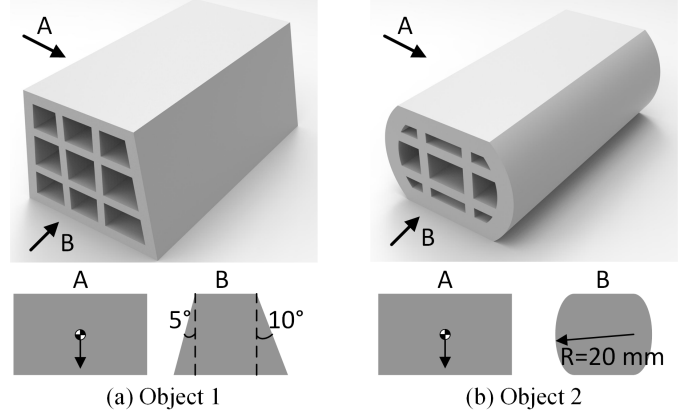


Fig. 12. Two different grasping items: (a) Asymmetric quadrilateral prism and (b) Curved objects.

The control diagram depicted in Fig. 11 outlines the control scheme utilized in the experiments. The Force Controller, implementing conventional PID control, is utilized to control the gripper and attain the desired grasping force. The input for this controller is the target force F_{target} , while the output is the distance x between two fingers. The PID parameters maintain the same values across all experiments. The Comparator is responsible for determining whether to engage the predicted grasping force. Operating with a threshold of 10%, its logic is as follows:

$$F_{\text{target}} = \begin{cases} 1.1 \tilde{F}_{\text{req}}, & \text{no prediction} \\ 1.1 \max(\tilde{F}_{\text{req}}, F_{\text{req}}), & \text{use prediction.} \end{cases} \quad (31)$$

A. Accuracy of Required Force Prediction

To comprehensively assess the accuracy of the minimum required grasping force prediction, we employed an asymmetrical trapezoidal column as the grasping object. Specifically, we selected positions that were deliberately offset from the center of mass to evaluate the applicability of the method in situations when torque is applied by the fingers. Additionally, we chose a curved object to grasp, as depicted in Fig. 12. The curvature radius of Object 2 (20 mm) was set to be smaller than the curvature radius of the fingers (39 mm).

To determine the friction coefficient, the following procedure was followed: (1) Apply a relatively small force to the object; (2) Move the finger nearly tangentially to induce slippage between the finger and the object; (3) Calculate the friction coefficient using the tangential and normal forces; (4) Repeat step (3) three times, averaging the results to obtain the measured friction coefficient. The relative slippage between fingers and objects can be very small, allowing the measurement of the coefficient of friction to be incorporated into each grip attempt. That is, in the subsequent grasping experiments, before grasping objects in subsequent experiments, a slight slippage between the fingers and the object is induced to measure the coefficient of friction.

Utilizing the method detailed in Algorithm (3), we calculated the minimum required grasping forces across various

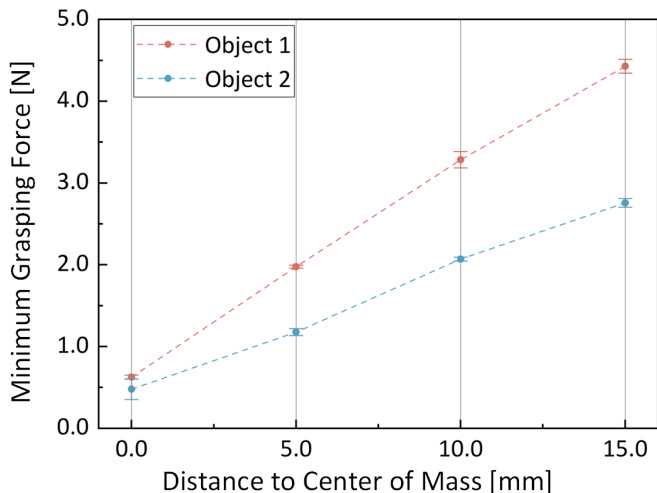


Fig. 13. Results for different grasping positions. The actual experiment was conducted five times at each position, and the predicted grasping forces were compared. And the mean and standard deviation of the error were calculated.

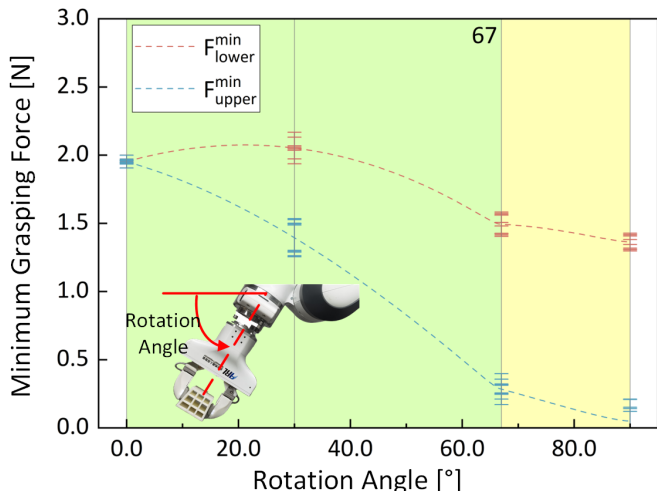


Fig. 14. Results for different rotation angles. Dashed lines represent results obtained using predictions. The green background indicates the prediction of the two-finger slip state, while the yellow background indicates the one-finger slip state.

positions and postures, subsequently comparing them with actual values obtained through the following steps: (1) Measure the friction coefficient between the object and the fingers; (2) Initiate the grasping process by applying a predetermined initial grip force and lifting the object off the ground; (3) Gradually reduce the applied grasping force until the object undergoes a slow sliding motion; (4) Utilize feedback from the tactile sensor to determine the actual minimum required grasping force; (5) Repeat the aforementioned steps five times and vary the given grasping positions or postures for each iteration.

As shown in Fig. 13, we first verified the accuracy of prediction on different position of Object 1. The error reaches its highest (0.13 N) when the distance to the center of mass is 10 mm. Additionally, to evaluate the error attributed to

assuming a flat contact surface in the required force solution, experiments were conducted on a curved object (Object 2). The tendency of the results is similar to those of Object 1, showing a rapid increase in minimum required grasping force as the grasping position moved away from the center of mass. The error reaches its highest (0.18 N) when the distance to the center of mass is 0. The green background in the figure represents the two-finger slip state, which is determined by the proposed method in Section V-D.

Furthermore, validation of required force prediction accuracy under varied postures was performed on Object 1, as depicted in Fig. 14. With an increase in the rotation angle θ , the grasping force for both fingers demonstrates a decreasing trend. The grasping force of the upper finger decreased at a faster rate. The yellow background indicates that at $\theta = 67^\circ$, the proposed method predicts the transition to a one-finger slip state. When the rotation angle is large, the upper finger tends to slip while the lower finger maintains stick to the object. The maximum prediction error for the minimum required grasping force was 0.16 N at $\theta = 90^\circ$ for the upper finger, and 0.12 N at $\theta = 30^\circ$ for the lower finger.

B. Adaptability of Required Force Prediction

To evaluate the applicability and computational efficiency of force prediction, we conducted simulation experiments on various objects commonly found in daily life. The method was implemented on a machine equipped with an AMD R7-5800H CPU (3.2 GHz), utilizing MATLAB without parallel runtime or GPU acceleration. For our analysis, we leveraged 3DNet [33], a repository containing virtual object models extensively employed in simulations [34]. Specifically, our analysis encompassed four typical items: the banana representing normal objects, the donut representing objects with holes, the bowl representing concave objects, the hammer representing tool objects, and the Stanford bunny representing complex objects. In the experiment, a large number of grasping positions were uniformly sampled on different objects. Algorithm 3 was then used to calculate the minimum grasping force required for objects at these various positions. The total time required for all positions was recorded, and the average time required for each grasping position was calculated based on the number of positions, as shown in Table II. For a specific grasping position, the required grasping force varies with changes in the object's posture. To maintain clarity, we kept the object's posture constant and set the grasping direction perpendicular to the y - z plane, as illustrated in Fig. 15.

We predefined the centers of mass for the objects and set the friction coefficient to 0.5. The results are presented in Fig. 16 and Table II. There are two important trends observed. Firstly, the magnitude of the grasping force is closely related to the distance between the grasping position and the center of mass. As the grasping position moves farther away from the center of mass, there is a tendency for the grasping force to increase. The most force-saving grasping positions for different objects typically reside near their respective centers of mass.

Secondly, the magnitude of the grasping force is also influenced by the orientation of the contact surface normal.

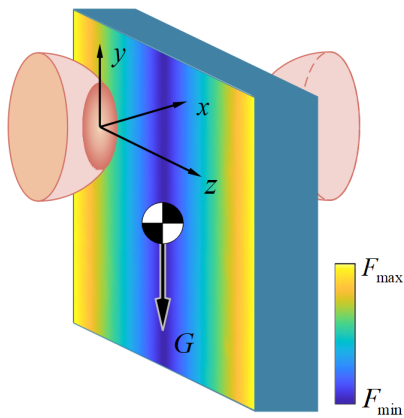


Fig. 15. Schematic diagram of the distribution of the minimum grasping forces. To enhance visual clarity, only two-dimensional distributions are shown.

TABLE II
SOLUTION TIME OF DIFFERENT OBJECTS

Objects	Points	Total Time [s]	Average Time [ms]
Banana	5122	134.3	26.2
Donut	8700	223.6	25.7
Bowl	7474	197.1	26.4
Hammer	4141	116.2	28.1
Bunny	4774	136.0	28.5

Taking the bowl as an example, For the grasping points near the edge of the bowl, even when they are far from the center of mass, the grasping force remains relatively low. This is because, compared to the inclined surface normal of the wall of the bowl, the flat platform at the mouth of the bowl is more conducive to the gripper exerting grasping force. At the same time, it is noticeable that the grasping force below the center of mass is relatively low compared to positions above the center of mass, indicating that the surface normal of the object being gripped does not necessarily need to be perfectly parallel to the gripping direction, but rather should have a certain angle with the gripping direction. This allows for better resistance against gravity for both normal and tangential forces at the contact point, potentially leading to a more force-efficient grasping position or posture.

C. Validation of the efficiency-improving method

To assess the effectiveness of required force prediction in enhancing grasping efficiency, we conducted grasping experiments using Object 1 at various grasping positions. In these experiments, an iron block was added to Object 1 to obscure its center of mass in the beginning. The experimental procedure followed the illustration in Fig. 9.

For the first grasping of the object, we employed a feedback-based force control strategy outlined as follows: (1) Measured the friction coefficient between the object and the fingers; (2) Initiated the grasp using a predetermined initial force; (3) Lifted the object at a specified lifting speed while concurrently measuring the current external wrench, using equations (3) and (4); (4) Utilized the method described in Algorithm (3) to determine the current minimum required grasping force; (5)

Controlled the grasping force to be higher than the minimum required grasping force by a certain threshold (set at 10%); (6) Continued lifting the object and adjusting the grasping force until it was successfully lifted off the ground; (7) Measured the center of mass of the object using the method described in Section IV-C.

Various lifting speeds were employed in the experiment, and the maximum lifting speed v_{\max} capable of successfully grasping the object was established. Throughout the experiment, data on the minimum required grasping force obtained from sensor feedback, the target grasping force set for the gripper, and the actual grasping force exerted by the gripper were recorded.

After determining the center of mass, the minimum required grasping force for a successful grasp was directly predicted. Using this value, we adjusted the initial grasping force. Subsequently, the object was lifted at a speed $v'_{\max} = 10 v_{\max}$. Similarly, the required grasping force, target grasping force, and actual grasping force were recorded. Our experiments were conducted at three different distances from the geometric center of the object. The results are illustrated in Fig. 17.

The experiment measured a lifting speed of $v_{\max} = 1 \text{ mm/s}$, thereby setting $v'_{\max} = 10 v_{\max} = 10 \text{ mm/s}$. As the grasping time prolongs with the object continuously being lifted, the required force exhibits a steady increase. Correspondingly, both the target force and actual force rise proportionately until the object is successfully lifted. The results of the feedback-based force control method without prediction are shown in the top row of Fig. 17. When the speed reaches the maximum successful grasping speed v_{\max} , the required force becomes close to the actual force in the lifting phase. This alignment suggests the object is prone to sliding, ultimately leading to grasping failure.

On the other hand, when adjusting the initial grasping force based on the experimentally obtained center of mass measurement, even with an escalated lifting speed at $v'_{\max} = 10 v_{\max}$, the actual grasping force consistently remains above a threshold higher than the minimum required grasping force. This assurance ensures the object remains undamaged and prevents slippage, facilitating stable and efficient grasping. It is observed that the threshold exceeds the preset value of 10%. This deviation could be due to the challenge of maintaining the object posture unchanged within the gripper when the predictive method is not employed. Although the method ensures no slippage between the fingers and the object, due to the tendency to slip and the elasticity of the soft fingers, the object is prone to rotate slightly under the influence of gravity. This rotation leads to a reduction in the torque exerted by gravity on the object, resulting in the gravity measurement error. This discrepancy is also evident in the force curves observed when employing the predictive method (lower row in Fig. 17): the required grasping forces exhibit varying degrees of increase in the beginning.

D. Adaptability of the efficiency-improving method

To assess the adaptability of the method across various objects, we conducted grasping experiments on 10 different

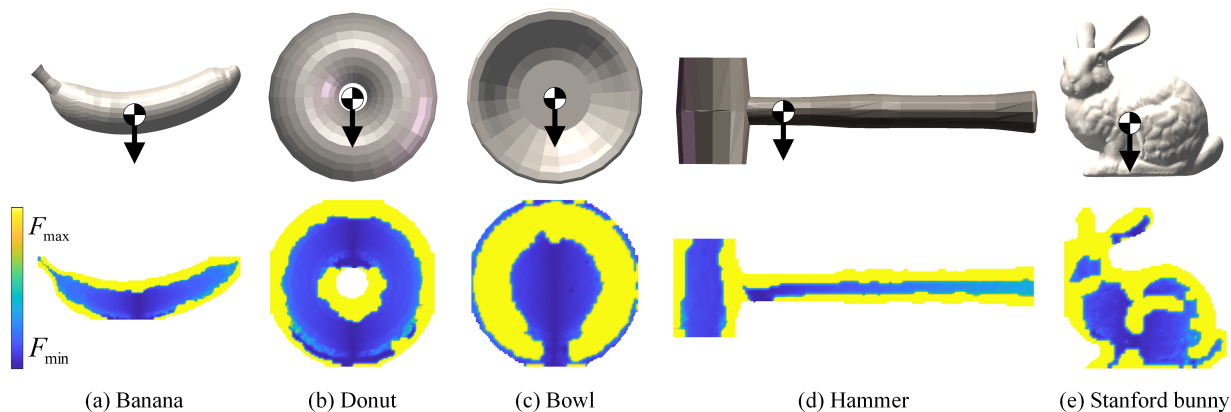


Fig. 16. Results for (a) Banana, (b) Donut, (c) Bowl, (d) Hammer, and (e) Stanford bunny are displayed. The yellow region represents the grasping points where the grasping force exceeds ten times the minimum grasping force or the object cannot be grasped.

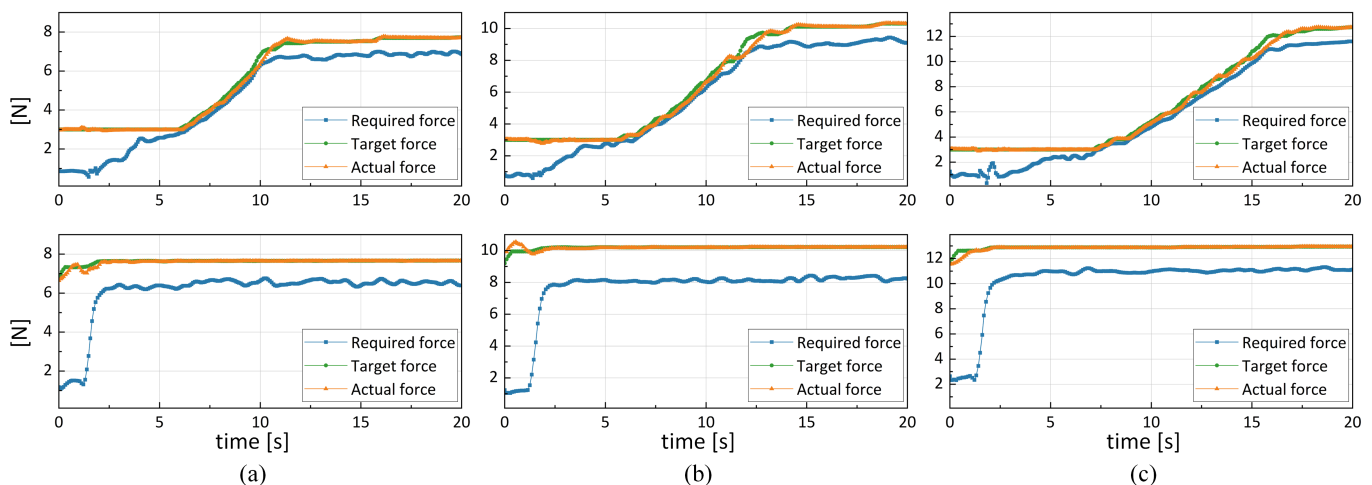


Fig. 17. Gripping force control curves at different positions, each at a distance of (a) 10 mm, (b) 15 mm, and (c) 20 mm from the center of mass. The top row depicts results without employing prediction, while the bottom row illustrates results when utilizing prediction.

natural objects depicted in Fig. 18. The maximum grasping force exerted by the gripper was set to 15 N.

For each object, the experimental procedure was as follows: (1) Measure the friction coefficient between the object and the fingers. (2) Employ the grasping strategy depicted in Fig. (9) by continuously sensing the required force and moment during the “lift” phase. Adjust the grasping force until the object is successfully lifted. The initial force is set to 2 N, and the lifting speed is set to 1 mm/s. The safety threshold is established at 10% higher than the desired grasping force. (3) Measure the gravity and the center of mass position using equations (7)–(10) and place the object back in its original position. (4) Generate the next grasping position randomly and predict the required grasping force using the method outlined in Algorithm (3). (5) Adjust the initial force to the predicted value and lift at a speed of 10 mm/s. (6) Repeat steps (4) and (5) a total of 10 times, and calculate the success rate. Due to the small differences in friction coefficients for the same object at different positions, we measured the friction coefficient only in the first grasping attempt and applied this measured value in subsequent grasps at different positions.

In the experiment, the randomly generated grasping positions are depicted in Fig. 18, and the robotic arm moves in the z-direction of the ground coordinate system. The range of random positions l_{range} is initially set based on the size of the object. Moreover, considering potential object localization errors resulting from vision-based object localization, the initial object position remains consistent across multiple grasping attempts. The relative position between the gripper and the object is acquired through feedback from the robotic arm.

The results are presented in Table III, where F_{max} denotes the maximum grasping force without crushing the object, and l_{range} denotes the range of randomly selected grasping position, with the center of mass as the origin. In the experiments, the required grasping force notably increases as the distance from the center of mass increases.

For both the champagne glass, the hammer, and the half-bottled juice, the success rate of grasping is influenced by the grasping range l_{range} . When the grasping position is too far away from the center of mass, the required grasping force may surpass the maximum capacity of the gripper, resulting

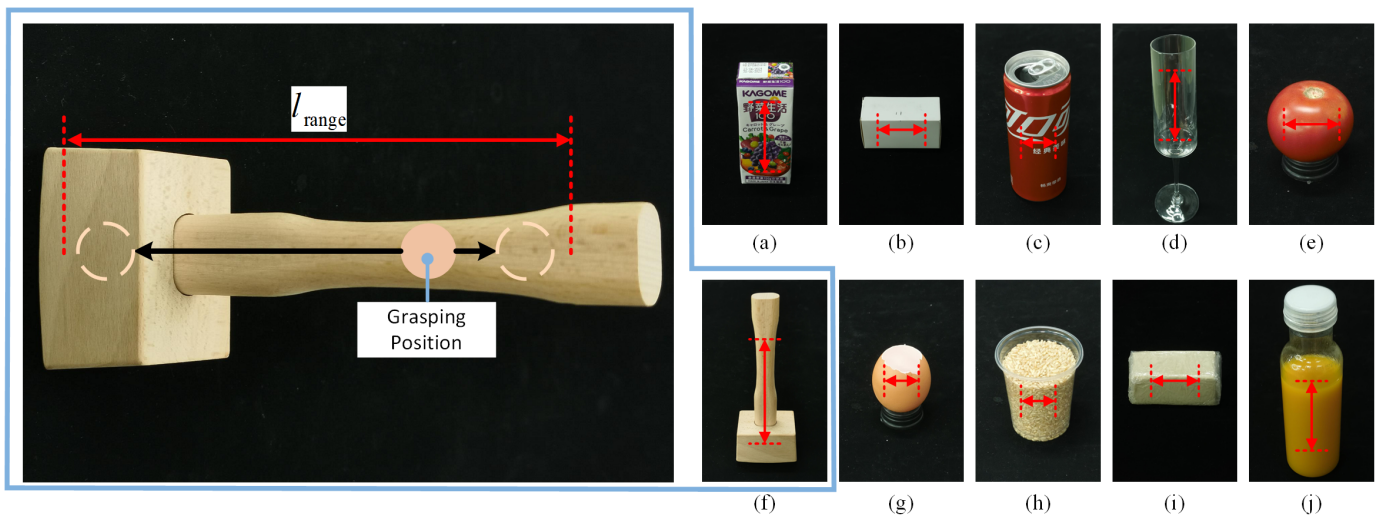


Fig. 18. Different objects from daily life and their relative postures to the gripper in the experiment. Each object will be randomly grasped within the grasping range l_{range} , with ten grasping attempts made for each object.

in slip failures. Restricting the grasping range near the center of mass ensures that the required force for successful grasping remains within the maximum capability of the gripper, leading to a notable improvement in the success rate.

Regarding the tofu, achieving successful grasping demands a higher precision in the grasping range due to its low tolerance for maximum grasping force. Without constraining the grasping range, there is a high likelihood of crushing the object. The revised l_{range} is determined using the algorithms proposed in this study, which computes the distance between the grasping position and the center of mass when the grasping force reaches the limit of the gripper or of the object, thereby establishing the range boundaries for random grasping positions.

For the half-bottled juice, even with modifications made to the grasping range l_{range} , there remains a probability of failure (20%). This probability arises because the internal juice can cause a shift in the center of mass with variations in the grasping position, resulting in a margin of error in predicting the required grasping force.

E. Demonstration Experiment

The experimental procedure for the demonstration experiments is illustrated in Fig. 19. The maximum safe grasping force F_{limit} is set at 10 N. The gripper sequentially grasp the objects in three different scenarios, and place them in designated locations, while recording the time required for each scenario. The grasping forces are controlled using three methods, respectively: (1) a predefined constant grasping force (5 N), set at half of the maximum safe force the object can withstand; (2) a pure feedback-based method; and (3) an approach that incorporates prediction into the feedback control process.

The final experimental results are summarized in Tab. IV. With a predefined and constant grasping force, grasping efficiency is relatively high; however, since the force may not

TABLE III
GRASPING RESULTS OF DIFFERENT OBJECTS.

Objects	μ	F_{max} [N]	l_{range} [mm]	Success Rate
Carton pack juice	1.17	12.4	[-40,40]	100%
Box with contents	1.04	> 15	[-20,40]	100%
Empty can	0.29	6.2	[-15,15]	100%
Ripe tomato	1.16	11.2	[-15,15]	100%
Half egg shelf	0.37	5.6	[-7.5,7.5]	100%
Plastic cup of rice	0.48	9.5	[-7.5,7.5]	100%
Champagne glass	0.70	> 15	[80,160] [80,90]	30% 100%
Hammer	1.14	> 15	[-15,160] [-15,15]	20% 100%
Tofu	0.70	3.2	[-20,20] [-3,3]	10% 100%
Half-bottled juice	2.03	> 15	[-20,80] [-20,50]	40% 80%

always meet the requirements, the success rate is not guaranteed. The pure feedback method yields a higher success rate but is limited in efficiency. In contrast, integrating prediction significantly enhances efficiency during subsequent regrasping compared to the feedback-based method. Additionally, the predictive approach allows for the assessment of whether the chosen grasping position can successfully grasp the object—ensuring that the required grasping force is less than both the maximum output force of the robotic hand and the object’s maximum tolerable force, thereby preventing failed grasping attempts. It is important to note that this prediction is based on the assumption of consistent friction coefficients across the object; if friction coefficients vary, it is necessary to measure the friction coefficients in advance.

VII. DISCUSSION

By adjusting the grasping force using predictions, the experimental findings suggest that stable grasping on various everyday objects remains achievable even when increasing the

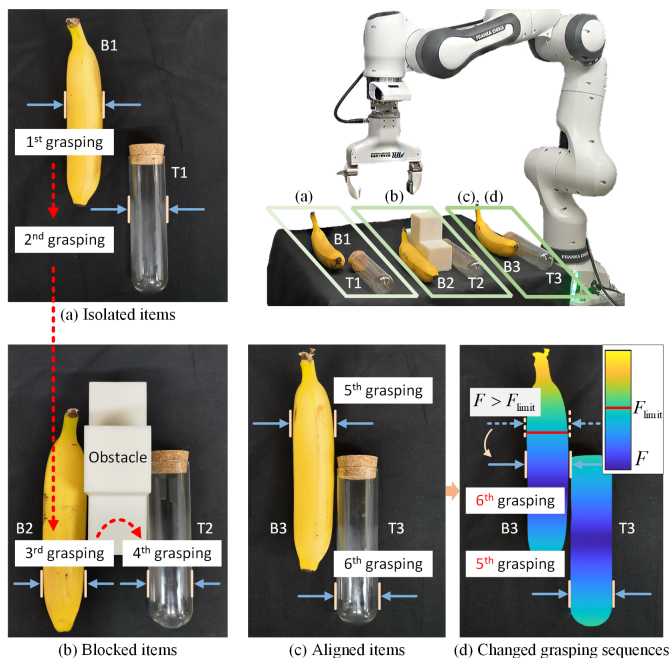


Fig. 19. The grasping positions and sequence for different scenarios.

TABLE IV
GRASPING TIME OF DIFFERENT METHODS

Methods	Isolated [s]		Blocked [s]		Aligned [s]	
	B1	T1	B2	T2	B3	T3
PF	5.8	5.8	Failed	5.6	Failed	6.4
FB	26.4	26.2	27.0	28.3	Failed	31.1
Ours	26.2	26.3	5.5	5.7	6.2	6.3

PF: Pre-set force; FB: Feedback-based force control

lifting speed to 10 times its original limit. After integrating force prediction, the grasping time has been reduced from 27.0 s to 6.3 s. Though assuming that the contact surface needs to be approximated as flat, the method still demonstrates good precision (0.18 N) when applied to surfaces with large curvature (curvature radius $20 \text{ mm} < \text{finger curvature radius } 39 \text{ mm}$). Moreover, the predictive algorithm for determining the required grasping force demonstrates robust applicability, effectively adapting to diverse and complex objects with varying shapes (with an average computation time of less than 29 ms). The results of the demonstration experiments show that incorporating prediction into the feedback process can reduce grasping time from 26.2 s to 6.3 s.

One significant source of accuracy error in determining the final force arises from assuming a central symmetric distribution of the pressure within the contact surface, as outlined in equation (33). The magnitude of this distributed normal force impacts both the resultant force and moment applied by the fingers to the object, thereby influencing the accuracy of grasping force prediction. Force distribution can be influenced by factors such as contact surface morphology and finger shape. To attain more precise force distribution characteristics, it would be beneficial to use sensors capable of measuring force distribution, such as the Tac3D [32] used

in this study, or other deformable sensors like GelSight [35].

Gripping force prediction relies on measuring the center of mass. For objects where the center of mass significantly shifts, such as containers with flowing liquids, the effectiveness of this method may be limited. Raising the safety threshold could be one way to make sure that the grasping force is still sufficient to meet the necessary requirements, even in cases when there is a certain amount of center of mass displacement. An alternative and efficient strategy could entail a heightened dependence on real-time measurements to consistently update the position of the center of mass.

The aim of predicting the minimum required grasping force is to prevent object slippage while avoiding damage. However, for heavy objects, the required grasping force might exceed the maximum capacity of the robotic hand. In such instances, it becomes essential to assess and filter grasping positions based on whether the required grasping force exceeds the limit of the gripper. Additionally, for certain off-center positions of delicate objects like tofu, the required grasping force might surpass the object's tolerance level, making successful grasping unfeasible without risking damage. To mitigate the risk of object damage, filtering grasping positions based on whether the grasping force exceeds the object's tolerance limit can be a promising approach.

VIII. CONCLUSION

Our method significantly improves grasping efficiency in handling unknown objects after the first successful grasping. By accurately predicting the required grasping force for grasping the object, our approach allows for quicker lifting of objects. In the dynamic process of grasping, interactions with the environment pose challenges in determining the appropriate grasping force, requiring continuous perception of the current state and adjustment of the grasping force. Our research reveals predicting the final required grasping force significantly reduces real-time perception of external forces, thereby further optimizing grasping efficiency.

Our approach outlines characteristics and methods for calculating and predicting the wrench required on the contact surface. This prediction assists in determining the current required grasping force. Once the finger material is given, key grasping information necessary for predicting the required grasping force includes the center of mass position, friction coefficient, and orientation of the contact surface. Moreover, we present a methodology for determining the minimum required grasping force for a parallel gripper considering soft fingertips. Establishing this minimum grasping force threshold holds significance in two-finger grasping as it serves to prevent object slippage. Additionally, this threshold stands as a novel evaluation metric used to assess grasping performance.

The success criterion for grasping in this study primarily is preventing the object from dropping, which further requires avoiding macro sliding between the object and the fingers. However, there are certain specific macro sliding conditions, such as rotational slippage, where the object may not necessarily fall from the hand but instead pivots within the

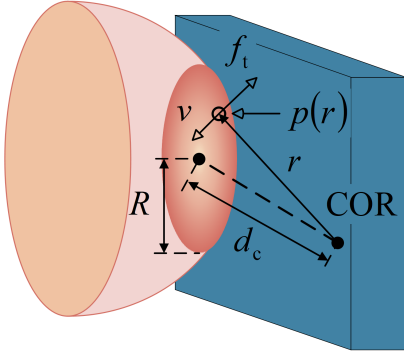


Fig. 20. The slip state of the soft finger contact, along with its center of rotation, determines the direction of the distributed tangential forces denoted as f_t .

grasp. Future research endeavors will further investigate the predictability of this rotational movement and its potential impact on the overall grasping process.

APPENDIX LIMIT SURFACE THEORY

When deformation is not negligible, a soft contact model should be considered, where the contact surface is no longer a single point. According to the theory and the experimental validation, the soft contact model can be categorized into the time-dependent model and the time-independent model. For the time-independent model, Xydias and Kao developed the power-law equation [22]:

$$R = cF_n^\gamma, \quad (32)$$

where R is the radius of the contact surface and F_n is the normal force and c is the coefficient depending on the size, shape of the fingertip, and material properties. $\gamma = n/(2n+1)$ is the exponent of the power-law equation with $n \in [0, 1]$ being the stress exponent for elastic materials. Apart from the time-independent model, another group is the time-dependent model or viscoelastic model. These models consider the creep and relaxation phenomena in soft materials [36]. Compared with the time-independent models, the viscoelastic models are more time-consuming.

The distribution of the pressure satisfies the following equation:

$$P(r) = C_k \frac{F_n}{\pi R^2} \left[1 - \left(\frac{r}{R} \right)^k \right]^{\frac{1}{k}}, \quad (33)$$

where k relates to the material of the fingertip and determines the shape of the pressure profile. C_k is used to adjust the pressure distribution to satisfy the equilibrium condition, where the integration of pressure over the contact surface equals the normal force N . C_k can be obtained as

$$C_k = \frac{3}{2} \frac{k\Gamma\left(\frac{3}{k}\right)}{\Gamma\left(\frac{1}{k}\right)\Gamma\left(\frac{2}{k}\right)} \quad (34)$$

where $\Gamma(\cdot)$ is the Gamma function. The coefficient with $k \geq 2$ are more common used pressure distributions.

When the fingertip slips relative to the object, there exists a center of rotation (COR) [37]. All points on the contact surface

of the finger rotate around the COR, with the axis of rotation perpendicular to the normal direction of the contact surface, as shown in Fig. 20. The direction of frictional force is inverted to the direction of relative motion and the tangential forces over the entire contact surface can be obtained by integrating the frictional forces over the infinitesimal surfaces:

$$F_t = \int \mu \frac{d \cos \theta - d_c}{\sqrt{d^2 + d_c^2 - 2dd_c \cos \theta}} P(r) dA, \quad (35)$$

where μ is the friction coefficient of the contact surface. d is the distance between the COR and the infinitesimal surface. Similarly, the normal moment can be obtained:

$$M_n = \int \mu \frac{d^2 - dd_c \cos \theta}{\sqrt{d^2 + d_c^2 - 2dd_c \cos \theta}} P(r) dA. \quad (36)$$

The joint (32)–(36) leads to the following conclusion: the tangential force and the normal moment are approximately distributed on an ellipse.

$$\frac{F_t^2}{F_{\max}^2} + \frac{M_n^2}{M_{\max}^2} = 1, \quad (37)$$

where $F_{\max} = F_t|_{d_c \rightarrow \infty} = \mu F_n$ and $M_{\max} = M_n|_{d_c=0}$ are the maximum tangential force and normal moment under the force F_n .

REFERENCES

- [1] R. S. Johansson and J. R. Flanagan, "Coding and use of tactile signals from the fingertips in object manipulation tasks," *Nat. Rev. Neurosci.*, vol. 10, no. 5, pp. 345–359, May 2009.
- [2] B. Zhang, Y. Xie, J. Zhou, K. Wang, and Z. Zhang, "State-of-the-art robotic grippers, grasping and control strategies, as well as their applications in agricultural robots: A review," *Comput. Electron. Agric.*, vol. 177, p. 105694, Oct. 2020.
- [3] R. Yagawa, R. Ishikawa, M. Hamaya, K. Tanaka, A. Hashimoto, and H. Saito, "Learning food picking without food: Fracture anticipation by breaking reusable fragile objects," in *Proc. IEEE Int. Conf. Robot. Autom.* London, United Kingdom: IEEE, May 2023, pp. 917–923.
- [4] H. Dang and P. K. Allen, "Stable grasping under pose uncertainty using tactile feedback," *Auton. Robot.*, p. 22, 2014.
- [5] F. Abi-Farraj, C. Pacchierotti, O. Arenz, G. Neumann, and P. R. Giordano, "A haptic shared-control architecture for guided multi-target robotic grasping," *IEEE Trans. Haptics*, vol. 13, no. 2, pp. 270–285, Apr. 2020.
- [6] Z. Xia, Z. Deng, B. Fang, Y. Yang, and F. Sun, "A review on sensory perception for dexterous robotic manipulation," *Int. J. Adv. Robot. Syst.*, vol. 19, no. 2, p. 172988062210959, Mar. 2022.
- [7] R. Sui, L. Zhang, Q. Huang, T. Li, and Y. Jiang, "A novel incipient slip degree evaluation method and its application in adaptive control of grasping force," *IEEE Trans. Autom. Sci. Eng.*, 2023.
- [8] H. Khamis, B. Xia, and S. J. Redmond, "Real-time friction estimation for grip force control," in *Proc. IEEE Int. Conf. Robot. Autom.* Xi'an, China: IEEE, May 2021, pp. 1608–1614.
- [9] J. W. James and N. F. Lepora, "Slip detection for grasp stabilization with a multifingered tactile robot hand," *IEEE Trans. Robot.*, vol. 37, no. 2, pp. 506–519, Apr. 2021.
- [10] R. Sui, L. Zhang, T. Li, and Y. Jiang, "Incipient slip detection method for soft objects with vision-based tactile sensor," *Measurement*, vol. 203, p. 111906, Nov. 2022.
- [11] M. T. Francomano, D. Accoto, and E. Guglielmelli, "Artificial sense of slip—a review," *IEEE Sensors J.*, vol. 13, no. 7, pp. 2489–2498, Jul. 2013.
- [12] J. Li, S. Dong, and E. Adelson, "Slip detection with combined tactile and visual information," in *Proc. IEEE Int. Conf. Robot. Autom.* Brisbane, QLD: IEEE, May 2018, pp. 7772–7777.
- [13] S. Dong, D. Ma, E. Donlon, and A. Rodriguez, "Maintaining grasps within slipping bounds by monitoring incipient slip," in *Proc. IEEE Int. Conf. Robot. Autom.* Montreal, QC, Canada: IEEE, May 2019, pp. 3818–3824.

- [14] F. Veiga, J. Peters, and T. Hermans, "Grip stabilization of novel objects using slip prediction," *IEEE Trans. Haptics*, vol. 11, no. 4, pp. 531–542, Oct. 2018.
- [15] M. Stachowsky, T. Hummel, M. Moussa, and H. A. Abdullah, "A slip detection and correction strategy for precision robot grasping," *IEEE/ASME Trans. Mechatron.*, vol. 21, no. 5, pp. 2214–2226, Oct. 2016.
- [16] Y. Kanakogi and S. Itakura, "Developmental correspondence between action prediction and motor ability in early infancy," *Nat. Commun.*, vol. 2, no. 1, p. 341, Jun. 2011.
- [17] N. Mavrakis and R. Stolkin, "Estimation and exploitation of objects' inertial parameters in robotic grasping and manipulation: A survey," *Robotics and Autonomous Systems*, vol. 124, p. 103374, Feb. 2020.
- [18] R. Calandra, A. Owens, M. Upadhyaya, W. Yuan, J. Lin, E. H. Adelson, and S. Levine, "The feeling of success: Does touch sensing help predict grasp outcomes?" Oct. 2017.
- [19] J. Xu, M. Danielczuk, E. Steinbach, and K. Goldberg, "6dfc: Efficiently planning soft non-planar area contact grasps using 6d friction cones," in *Proc. IEEE Int. Conf. Robot. Autom.* Paris, France: IEEE, May 2020, pp. 7891–7897.
- [20] D. Pretorius and C. Fisher, "A novel method for computing the 3d friction cone using complimentary constraints," in *Proc. IEEE Int. Conf. Robot. Autom.* Xi'an, China: IEEE, May 2021, pp. 5000–5006.
- [21] A. Fakhari, M. Keshmiri, and I. Kao, "Development of realistic pressure distribution and friction limit surface for soft-finger contact interface of robotic hands," *J. Intell. Robot. Syst.*, vol. 82, no. 1, pp. 39–50, Apr. 2016.
- [22] N. Xydias and I. Kao, "Modeling of contact mechanics and friction limit surfaces for soft fingers in robotics, with experimental results," *Int. J. Rob. Res.*, vol. 18, no. 9, pp. 941–950, Sep. 1999.
- [23] A. Fakhari, I. Kao, and M. Keshmiri, "Modeling and control of planar slippage in object manipulation using robotic soft fingers," *ROBOMECH J.*, vol. 6, no. 1, p. 15, Dec. 2019.
- [24] J. Xu, T. Aykut, D. Ma, and E. Steinbach, "6dls: Modeling nonplanar frictional surface contacts for grasping using 6-d limit surfaces," *IEEE Trans. Robot.*, vol. 37, no. 6, pp. 2099–2116, Dec. 2021.
- [25] M. Costanzo, G. De Maria, and C. Natale, "Two-fingered in-hand object handling based on force/tactile feedback," *IEEE Trans. Robot.*, vol. 36, no. 1, pp. 157–173, Feb. 2020.
- [26] Z. Pan, X. Gao, and D. Manocha, "Grasping fragile objects using a stress-minimization metric," in *Proc. IEEE Int. Conf. Robot. Autom.* Paris, France: IEEE, May 2020, pp. 517–523.
- [27] L. He, Q. Lu, S.-A. Abad, N. Rojas, and T. Nanayakkara, "Soft fingertips with tactile sensing and active deformation for robust grasping of delicate objects," *IEEE Robot. Autom. Lett.*, vol. 5, no. 2, pp. 2714–2721, Apr. 2020.
- [28] K. Tai, A.-R. El-Sayed, M. Shahriari, M. Biglarbegian, and S. Mahmud, "State of the art robotic grippers and applications," *Robotics*, vol. 5, no. 2, p. 11, Jun. 2016.
- [29] L. Birglen and T. Schlicht, "A statistical review of industrial robotic grippers," *Robot. Comput. Integr. Manuf.*, vol. 49, pp. 88–97, Feb. 2018.
- [30] M. Suomalainen, Y. Karayiannidis, and V. Kyrki, "A survey of robot manipulation in contact," *Rob. Auton. Syst.*, vol. 156, p. 104224, 2022.
- [31] J. J. Moré, "The levenberg-marquardt algorithm: Implementation and theory," in *Numerical Analysis*, G. A. Watson, Ed. Berlin, Heidelberg: Springer Berlin Heidelberg, 1978, pp. 105–116.
- [32] L. Zhang, T. Li, and Y. Jiang, "Improving the force reconstruction performance of vision-based tactile sensors by optimizing the elastic body," *IEEE Robot. Autom. Lett.*, vol. 8, no. 2, pp. 1109–1116, Feb. 2023.
- [33] W. Wohlkinger, A. Aldoma, R. B. Rusu, and M. Vincze, "3dnet: Large-scale object class recognition from cad models," in *Proc. IEEE Int. Conf. Robot. Autom.* St Paul, MN, USA: IEEE, May 2012, pp. 5384–5391.
- [34] R. Newbury, M. Gu, L. Chumbley, A. Mousavian, C. Eppner, J. Leitner, J. Bohg, A. Morales, T. Asfour, D. Kragic, D. Fox, and A. Cosgun, "Deep learning approaches to grasp synthesis: A review," 2022.
- [35] A. C. Abad and A. Ranasinghe, "Visuotactile sensors with emphasis on gelsight sensor: A review," *IEEE Sensors J.*, vol. 20, no. 14, pp. 7628–7638, Jul. 2020.
- [36] P. Tiezzi and I. Kao, "Modeling of viscoelastic contacts and evolution of limit surface for robotic contact interface," *IEEE Trans. Robot.*, vol. 23, no. 2, pp. 206–217, Apr. 2007.
- [37] S. Goyal, A. Ruina, and J. Papadopoulos, "Limit surface and moment function descriptions of planar sliding," in *Proc. IEEE Int. Conf. Robot. Autom.* Scottsdale, AZ, USA: IEEE Comput. Soc. Press, 1989, pp. 794–799.